How perfect is the Himalayan arc?

R. Bendick
R. Bilham
Cooperative Institute for Research in Environmental Sciences (CIRES), University of Colorado, Boulder, Colorado 80309-0399, USA

ABSTRACT

The Himalayan plate boundary, because it is entirely subaerial, is both the most dramatic and the most accessible to direct observation of all active convergent boundaries on Earth. The shape of this boundary can be described as a small circle of radius 1696 ± 55 km, centered at long 91.6° ± 1.6°E and lat 42.4° ± 2.1°N for the extent of the arc between long 77.2° and 92.1°E. The pole of this small circle is consistent whether seismicity, topography, or stress state is used to define the position of the tectonic boundary. The defined small circle also coincides with a peak in microseismicity, the maximum horizontal strain rate, and a peak in the vertical velocity field. This quantitative definition of a stable, curved tectonic boundary is a prerequisite to modeling the dynamics of curvature in convergent arcs and applying appropriate boundary conditions to other regional models.

Keywords: convergence, arcs, tectonics, geomorphology, Himalaya.

INTRODUCTION

One of the common characteristics of convergent boundaries worldwide is a curved shape. Such curvature has been included in the analyses of the Aleutian arc (Avé-Lallemant, 1996), South America (Judge and McNutt, 1991), and the Himalaya (Royden and Burchfiel, 1987), among others (e.g., McCaffrey, 1996), but has not been explicitly quantified for these locations. The Himalayan arc appears to be in a steady-state equilibrium condition with respect to shape in map view, independent of topographic steady state discussed for mountain ranges elsewhere (e.g., Dahlen, 1990). Such equilibrium requires a mechanism. We propose a formal analogy with the interfacial forces of surface thermodynamics, the further development of which requires the rigorous definition of a geometric and physical interface. Thus, although several attempts have been made to describe the dynamics of curvature at collisions (e.g., Buck and Sokoutis, 1994; Bevis, 1986; Frank, 1968; Tanimoto, 1998), we consider it necessary to first demonstrate that: (1) at least one collisional boundary is curved, according to a simple geometrical rule, (2) the curvature is consistent among several independent types of data used to delineate tectonic boundaries, and therefore (3) a simple, coherent tectonic interface may be described. The India-Asia collision is especially suited to such an investigation because topographic and velocity data are distributed throughout the deforming region such that description of the shape is not influenced by the spatial distributions of measurements, as might be the case for arcs where most of the deforming region is submarine.

This paper is divided into three parts. In the first, data with broad distribution along the Himalayan arc are used to define small-circle approximations of the plate boundary. In the second, additional data with incomplete along-arc coverage are analyzed for agreement with the previously estimated small circle. We then discuss the implications of a geometrically coherent boundary on the regional dynamics.

The data used for the curve-fitting analysis include the world 30′ data set (GTOPO30; Eros Data Center, 1996), seismicity from the Engdahl–van der Hilst–Buland catalog (Engdahl et al., 1998) and from Molnar and Lyon-Caen (1989), fluvial geomorphology (Seeber and Gornitz, 1983), and change in stress state due to topographic loading (e.g., Mercier et al., 1987; Armijo and Tapponnier, 1989). Supporting but incomplete data include horizontal and vertical velocity measurements from the global positioning system (GPS), fault kinematics, and leveling.

Additional qualitative data demonstrate that the rheologies of the Indian subcontinent and the Tibetan Plateau differ and that the transition between the two occurs across the narrow arcuate zone of the Himalaya. Principal stress directions inferred from seismicity and borehole measurements (Zoback, 1992) appear to rotate to remain arc normal within the arc, and the minimum compressive stress changes from vertical on the Indian craton to horizontal in Tibet. Temperature from heat-flow measurements (Francheteau et al., 1984; Gupta and Yamano, 1995) and rigidity from seismic tomography (Brown et al., 1996) suggest a cold, rigid India and a soft, hot Tibet.

REGIONAL OBSERVATIONS

Topography

The analysis of relief in this section is predicated on the assumption that maximum relief in the Himalaya corresponds to maximum vertical velocity of particles in the deforming range. Relief depends on the interaction of uplift and fluvial incision, such that locations where uplift rates are high also have increased relief. This depends on the concomitant assumption that incision rates are approximately constant in arc-normal sections, such that incision is not the cause of variation in relief. In the one location where quantitative measurements of uplift rates from leveling exist, we confirm that the maximum relief and maximum vertical velocity are coincident (Bilham et al., 1997) (Fig. 1).

ArcInfo (ESRI, 1998) was used to convert the 30′ digital elevation model for Asia into a map of regional relief by application of filters at two wavelengths, 50 and 25 km. Trans-Himalayan arc-normal sections were then approximated by a Gaussian curve derived from a least-squares fit to the data. From these Gaussian curves, we were able to specify the form of relief in terms of four parameters: amplitude, wavelength, arc-normal location of maximum relief, and an elevation offset. The position of the Gaussian maximum was then used as the position of maximum relief for fitting a small circle (Fig. 2A).

Fits to subsegments of the arc were also made to search for scaling effects and along-arc shape variations. From these fits, we calculate that the line of maximum relief deviates by more than 2 σ from the small-circle approximation west of 74.9°E and east of 90.1°E. The length of the arc that conforms to a small-circle approximation is thus more than 1800 km. In the east, the divergence from the model arc seems to coincide with the Shillong Plateau, which may be accommodating large amounts of shortening south of the Himalaya (Bilham and England, 2001).

For circles fitted to varying arc lengths, all convergent solutions for the 50 km filter (Fig. 2A) range between lat 40.45°N and 42.3°N, between long 89.5°E and 90.9°E, and between radii of 1444 and 1688 km. This result suggests a real pole solution of $\theta = 41.6° \pm 0.8°$N, $\varphi = 90.3° \pm 0.8°$E, and $r = 1588 \pm 100$ km for the long-wavelength relief (Fig. 3). For the calculations using a filter with a radius of 25 km, the same methods give $\theta = 44.8° \pm 0.45°$N, $\varphi = 92.3° \pm 0.67°$E, and $r = 1955 \pm 66$ km (Fig. 3). It is clear that there are aliasing effects due to the sampling wavelength, but the results are remarkably consistent within the arc region.

All model small circles between long 74.9°E and 90.1°E are within a region with an

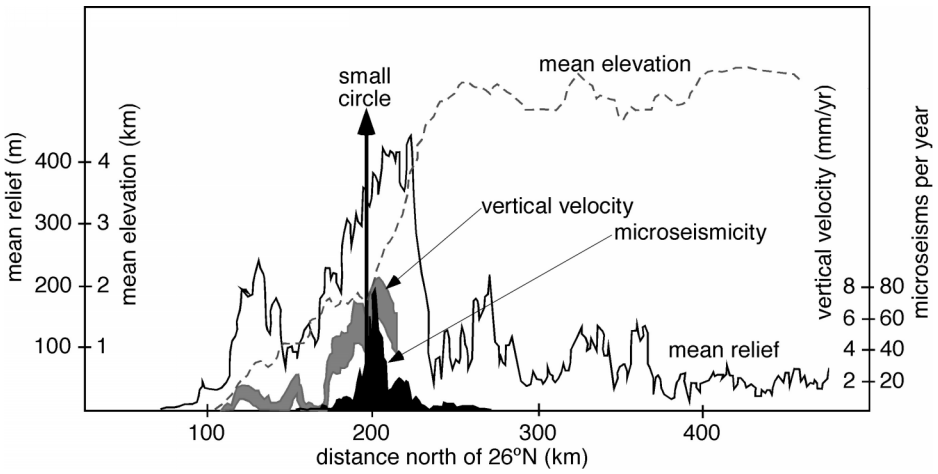

Figure 1. Plots of mean elevation, mean relief, vertical velocity with 1 σ error envelope, and microseismicity cross sections in arc-normal direction. All data used to construct these profiles were first straightened by projection, so that mathematical operations could combine cross sections throughout region. Peaks in vertical velocity and relief are coincident, suggesting that maximum relief elsewhere in arc may be used as proxy for position of maximum vertical velocity (modified from Bilham et al., 1997).

arc-normal width of only 18 km (Table 1; Fig. 3). The maximum deviation of maximum relief from the small-circle fit to the arc is only 48 km for the central 1800 km of the arc. Maximum misfits to the arc occur near the drainage basins of large trans-Himalayan rivers such as the Sutlej and the Karnali, where the quality of the Gaussian fits to trans-Himalayan relief is poor. If these data are omitted, maximum relief deviates from a small circle by less than 5 km in the central 1500 km of the Himalayan arc.

Seismicity

All events in the catalog of Engdahl et al. (1998) within the box between 25°N and 42°N and 70°E and 100°E and with focal mechanisms either in the Harvard CMT catalog (Centroid Moment Tensor Project, 2000) or in Molnar and Lyon-Caen (1989) were used in this analysis. Only 221 reverse events and 110 normal events had published mechanisms (Fig. 2B). The focal mechanisms were used to classify the fault motions; the epicenters from Engdahl et al. (1998) were used to map events. A small circle was then fit to all of the shallow, arc-normal thrust events. For circles fitted to varying arc lengths, all convergent solutions range between lat 40.6°N and 42.5°N, between long 92.1°E and 93.8°E, and between radii of 1557 and 1757 km. This result suggests a pole solution of $\theta = 41.6° \pm 1°$N, $\varphi = 92.7° \pm 1°$E, and $r = 1672 \pm 100$ km (Fig. 3).

Geomorphology

Seeber and Gornitz (1983) used digitized 1:1 000 000 and 1:250 000 topographic maps of the Himalayan arc to calculate arc-normal river-long profiles, the elevation of points along the main channel of the largest trans-Himalayan rivers. They argued that knick-

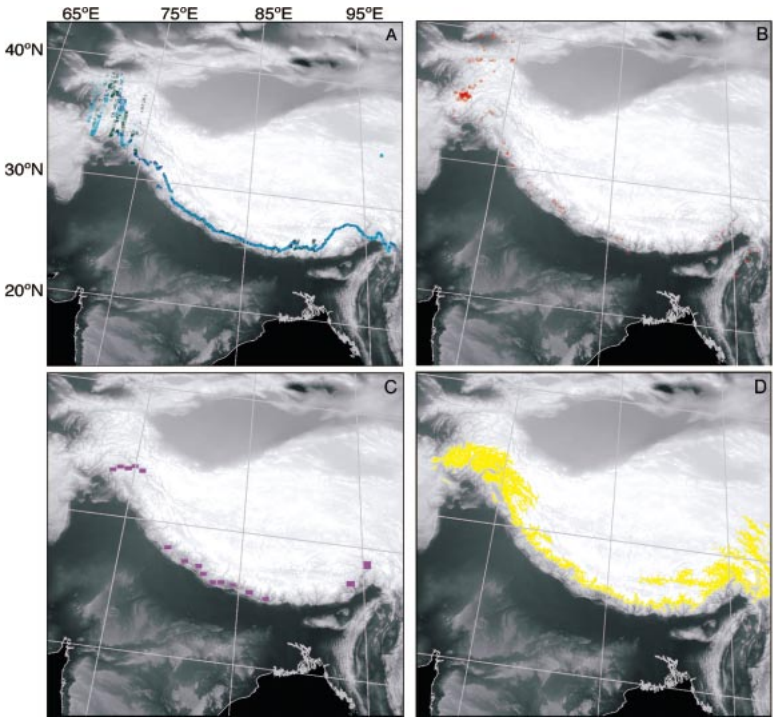

Figure 2. Input data for circle-fitting experiments. See text for discussion. A: Locations of maxima of Gaussian approximations of relief with 50-km-radius (light blue) and 25-km-radius (dark green) filter. B: Locations of 221 reverse seismic events with published hypocenters and focal mechanisms (Engdahl et al., 1998; Centroid Moment Tensor Project, 2000; Molnar and Lyon-Caen, 1989). C: Locations of reaches where Seeber and Gornitz (1983) estimated that river-long profiles are 10 times steeper than predicted. D: Location of 4000 m contour, approximate position of change in regional stress state. Figures 2–4 show topography projected onto best-fit pole to Himalaya.

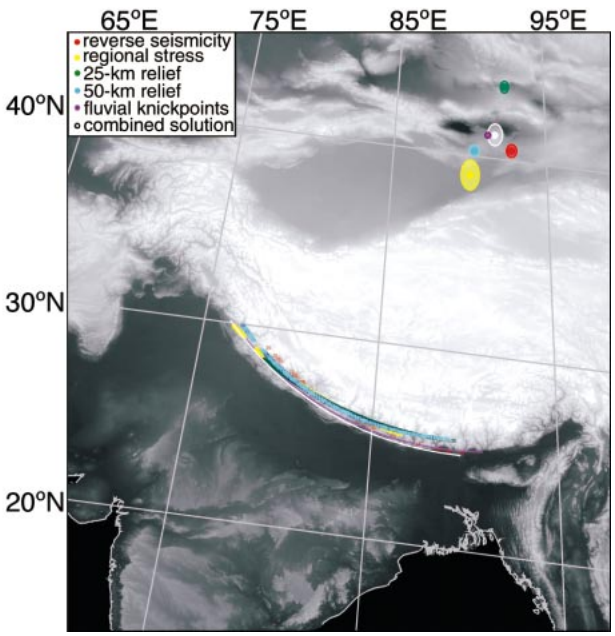

Figure 3. Best-fit small circles and poles with error ellipses. For central Himalaya, all small circles are statistically identical. We consider this result to demonstrate that (1) Himalayan boundary may be approximated as small circle with center of long 91.6°E, lat 42.4°N, and radius of 1696 km (combined solution), and (2) location of boundary is not sensitive to data type.

TABLE 1. RESULTS FROM FITTING A SMALL CIRCLE (IN A LEAST-SQUARES SENSE) TO DATA DESCRIBING THE HIMALAYAN ARC

Data set	Min. long. (°E)	Max. long. (°E)	r (km)	θ	φ	χ^2
Reverse*	75.315	92.761	1695.7	41.749	92.412	0.027
Reverse*	73.780	93.744	1555.6	40.556	92.074	0.058
Reverse*	73.320	94.278	1763.3	42.472	93.770	0.106
50 km λ†	74.478	85.942	1453.5	40.455	89.525	0.060
50 km λ†	71.390	85.942	1713.3	42.499	91.140	0.112
50 km λ†	71.390	88.806	1663.9	42.269	90.585	0.225
25 km λ§	70.002	94.506	2000.5	45.080	93.215	3.703
25 km λ§	74.490	90.786	1994.0	45.202	92.040	0.846
25 km λ§	78.594	88.802	1933.2	44.549	91.633	0.099
Fluvial#	——	——	1695.3	42.450	91.100	——
4000 m**	76.249	86.087	1124.3	37.672	87.978	0.372
4000 m**	78.002	84.958	2109.8	45.635	93.565	0.114
4000 m**	76.404	86.700	1174.7	38.065	88.398	0.419

Note: Subsegments of the data are fitted to test for scaling effects in the analysis.
*Reverse data are geographic positions of reverse seismic events with published hypocenters and focal mechanisms (Engdahl et al., 1998; Molnar and Lyon-Caen, 1989; Centroid Moment Tensor Project, 2000).
†50 km λ data are geographic positions of Gaussian maxima of topography filtered with a 50-km-radius relief filter.
§25 km λ data are Gaussian maxima of topography filtered with a 25-km-radius filter.
#Fluvial data are positions of oversteepened river reaches reported in Seeber and Gornitz (1983).
**4000 m data are geographic positions of the 4000-m-elevation contour.

points, convex reaches in otherwise concave fluvial profiles, represent the location of active uplift at rates exceeding the erosive power of the stream. These locations therefore represent maxima in the vertical velocity field (Fig. 2C). They fit a small circle centered at 42.45°N and 91.10°E with a radius of 1695 km (Fig. 3) to these oversteepened reaches.

Stress State

Several arguments have been made to demonstrate that India and Tibet have different stress regimes, notably that σ_1 and σ_3 swap directions across the High Himalaya (e.g., Mercier et al., 1987). South of the Tibetan Plateau, the maximum compressive stress (σ_1) is parallel to India-Asia convergence. Thrusting and vertical deformation are energetically favorable because the minimum stress direction (σ_3) is vertical. In the plateau, however, because of the gravitational potential of the elevated mass, the maximum compressive stress is vertical, and the minimum stress direction is approximately east-west. Thus, south of the plateau edge, the regime is dominantly north-south compression; within the southern plateau, the regime is dominantly east-west extension. The absolute magnitude of the compressive stress between India and Asia is not known, so the location at which the maximum vertical stress (which may be calculated simply as ρgh, where ρ is the average density of a column of crust, g is the acceleration of gravity, and h is the height of the crustal column) exceeds the compressive stress is not known. However, earthquake focal mechanisms (Molnar and Lyon-Caen, 1989) suggest that this transition occurs near the edge of the Tibetan Plateau, as approximated by the 4000 m contour (Fig. 2D). A small-circle fit to the smoothed 4000 m contour gives a pole very close to the pole from the maximum-relief calculations, but with a smaller radius. For circles fitted to varying arc lengths, all convergent solutions range between lat 37.67°N and 45.64°N, between long 87.98°E and 93.56°E, and between radii of 1124 and 2110 km. This result suggests a pole solution of $\theta = 40.46° \pm 3°$N, $\varphi = 89.98° \pm 2°$E, and $r = 1470 \pm 333$ km (Fig. 3).

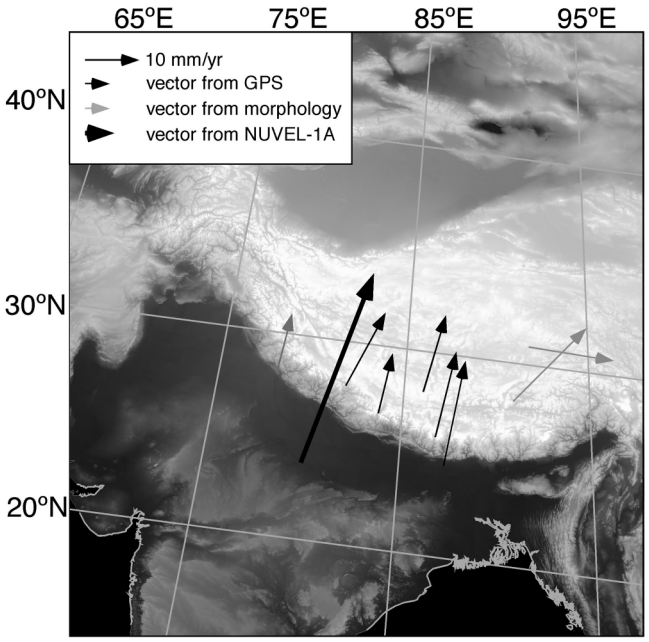

Figure 4. Regional velocity vectors have radial components. Estimates of arc-parallel stretching range from 4.5 ± 3.5 mm/yr (Jouanne et al., 1999) to 14 ± 2 mm/yr (Chen et al., 2000). Global positioning system (GPS) vectors are modified from Jouanne et al. (1999), Chen et al. (2000), and Larson et al. (1999). Vectors from offset terraces and moraines are from Wesnousky et al. (1999), Armijo and Tapponnier (1989), and Armijo et al. (1986). NUVEL-1A vector is from DeMets et al. (1994).

Velocity

The vertical motion of the collision zone is estimated in an analysis of leveling data from 1977 and 1995 by Jackson and Bilham (1994). At long 86°E, they identified a 40-km-wavelength region with a peak uplift of 7 ± 3 mm/yr relative to the India border. The point of maximum vertical velocity is centered at lat 27.9°N (Fig. 1). This direct measurement of maximum vertical velocity is coincident with the band of maximum vertical velocity estimated according to maximum relief.

Figure 4 summarizes values for horizontal-velocity vectors in the India-Asia collision zone as reported in the literature. GPS velocities are shown (e.g., Larson et al., 1999; Jouanne et al., 1999), as well as ground-based analysis of fault offsets and velocities (Armijo and Tapponnier, 1989; Armijo et al., 1986; Wesnousky et al., 1999). The salient feature of these point-velocity measurements is that they are not parallel to each other or to the total relative plate motion between India and Eurasia (DeMets et al., 1994). Rather, throughout the Himalayan boundary region, the horizontal-velocity vectors are rotated to arc normal (Fig. 4). This finding allows two conclusions: (1) one can begin to estimate a pole for these velocities, and (2) the pole represents an apparent pole of extrusion of the arc, such that there is an along-arc component of extension. Estimates of the magnitude of this along-arc extension range from 4.5 ± 3.5 mm/yr (Jouanne et al., 1999) to 14 ± 2 mm/yr (Chen et al., 2000).

Because velocity measurements within the Himalaya are concentrated in the center for the arc, the pole is poorly determined at this time. A small-circle approximation for the velocity-defined plate boundary, from the assumption that the convergence direction is arc normal and the extension direction is tangential, gives a center at lat 57° ± 19°N and long 98° ± 23°E.

Summary

Table 1 summarizes the results of modeling the shape of the boundary from relief, topographically derived stress, geomorphic, and seis-

mic data. Figure 3 shows a plot of all of the calculated poles with their error ellipses. The arcs derived from these pole solutions do not differ statistically within the central Himalaya.

DISCUSSION

The weighted combined results from the fitting of small circles to geographically distributed data give a powerful means of describing Himalayan geometry. Weighting is according to the standard deviation of the fit. The two-dimensional model of the boundary is best described as an arc of a circle with a center at lat 42.4° ± 2.1°N, long 91.6° ± 1.6°E, and a radius of 1696 ± 55 km between long 77.2°E and 92.1°E. This corresponds to an arc length of 0.28 radians (16.2° or 1800 km). Therefore, we conclude that the plate boundary may be approximated by this small circle both in models that require an appropriate boundary condition and in future efforts to explain the dynamics of the curvature of the collision process. Any dynamic model of collision must include a mechanism for producing and maintaining a small-circle form for the Himalaya.

The apparently stable condition of this arc, as suggested by the regional velocity and stress fields oriented so as to maintain an arcuate shape regardless of total convergence, suggests that the regional dynamics are related to the shape of the arc. Hitherto the form of the arc has been ascribed to the interaction of the east-west extension of Tibet with the northeast-directed convergence of India with Asia. Implicit in this explanation is that an along-arc tensile strain or extensional strain maintains the shape of the Himalaya. Previous suggestions for the origin of along-arc extension include gravitational collapse (Royden and Burchfiel, 1987; Buck and Sokoutis, 1994), partitioning effects (McCaffrey, 1996), and variations in elastic thickness along strike (Judge and McNutt, 1991). However, these mechanisms are ad hoc, and require special conditions in time and space to maintain a small-circle shape. We are currently developing an alternative mechanism: that the presence of an interface separating viscous sheets of differing strengths produces an interfacial force that may be modeled by using a formalism developed for surface tension. Such a mechanism produces a small circle without special starting conditions or boundary conditions, simply because the special case of equal Gaussian and mean curvatures is the minimum energy configuration for such a boundary.

REFERENCES CITED

Armijo, R., and Tapponnier, P., 1989, Late Cenozoic right-lateral strike-slip faulting in southern Tibet: Journal of Geophysical Research, v. 94, p. 2787–2838.

Armijo, R., Tapponnier, P., Mercier, J., and Tong-Lin, H., 1986, Quaternary extension in southern Tibet: Field observations and tectonic implications: Journal of Geophysical Research, v. 91, p. 13 803–13 872.

Avé-Lallemant, H., 1996, Displacement partitioning and arc-parallel extension in the Aleutian volcanic island arc: Tectonophysics, v. 256, p. 279–293.

Bevis, M., 1986, The curvature of Wadati-Benioff zones and the torsional rigidity of subducting plates: Nature, v. 323, p. 52–53.

Bilham, R., and England, P., 2001, The Shillong Plateau: A large-scale popup feature: Nature (in press).

Bilham, R., Larson, K., Freymueller, J., and Project Idylhim, 1997, GPS measurements of present-day convergence across the Nepal Himalaya: Nature, v. 386, p. 61–64.

Brown, L., Zhao, W., Nelson, K., Hauck, M., Alsdorf, D., Ross, A., Cogan, M., Clark, M., Liu, X., and Che, J., 1996, Bright spots, structure, and magmatism in southern Tibet from INDEPTH seismic reflection profiling: Science, v. 274, p. 1688–1690.

Buck, W.R., and Sokoutis, D., 1994, Analogue model of gravitational collapse and surface extension during continental convergence: Nature, v. 369, p. 737–740.

Centroid Moment Tensor Project, 2000, http://www.seismology.harvard.edu/CMTsearch.html (September 2000).

Chen, Q., Freymueller, J., Xu, C., Jiang, W., Yang, Z., and Liu, J., 2000, Active deformation in southern Tibet measured by GPS: Eos (Transactions, American Geophysical Union), v. 81, p. 183.

Dahlen, F., 1990, Critical taper model of fold-and-thrust belts and accretionary wedges: Annual Review of Earth and Planetary Sciences, v. 18, p. 55–99.

DeMets, C., Gordon, R.G., Argus, D.F., and Stein, S., 1994, Effect of recent revisions to the geomagnetic reversal time scale on estimates of current plate motions: Geophysical Research Letters, v. 21, p. 2191–2194.

Engdahl, R., van der Hilst, R., and Buland, R., 1998, Global teleseismic earthquake relocation with improved travel times and procedures for depth determination: Seismological Society of America Bulletin, v. 88, p. 722–743.

Eros Data Center, 1996, GTOPO30: Sioux Falls, South Dakota, U.S. Geological Survey, CD-ROM.

ESRI, 1998, ArcInfo software: Redlands, Washington, Environmental Systems Research Institute.

Francheteau, J., Jaupart, C., Shen, X., Kang, W., Lee, D., Bai, J., Wei, H., and Deng, H., 1984, High heat flow in southern Tibet: Nature, v. 307, p. 32–36.

Frank, F., 1968, Curvature of island arcs: Nature, v. 22, p. 363.

Gupta, M., and Yamano, M., 1995, Terrestrial heat flow in Asia: New Delhi and Oxford, IBH Publishing, Inc., 400 p.

Jackson, M., and Bilham, R., 1994, Constraints on Himalayan deformation inferred from vertical velocity fields in Nepal and Tibet: Journal of Geophysical Research, v. 99, p. 13 897–13 912.

Jouanne, F., Mugnier, J., Pandey, M., Gamond, J., LeFort, P., Serrurier, L., Vigny, C., and Avouac, J.-P., 1999, Oblique convergence in the Himalayas of western Nepal deduced from preliminary results of GPS measurements: Geophysical Research Letters, v. 26, p. 1933–1936.

Judge, A., and McNutt, M., 1991, The relationship between plate curvature and elastic plate thickness: A study of the Peru-Chile trench: Journal of Geophysical Research, v. 96, p. 16 625–16 639.

Larson, K., Burgmann, R., Bilham, R., and Freymueller, J., 1999, Kinematics of the India-Asia collision zone from GPS measurements: Journal of Geophysical Research, v. 104, p. 1077–1093.

McCaffrey, R., 1996, Estimates of modern arc-parallel strain rates in forearcs: Geology, v. 24, p. 27–30.

Mercier, J.-L., Armijo, R., Tapponnier, P., Carey-Gailhardis, E., and Lin, H., 1987, Change from late Tertiary compression to Quaternary extension in southern Tibet during the India-Asia collision: Tectonics, v. 6, p. 275–304.

Molnar, P., and Lyon-Caen, H., 1989, Fault plane solutions of earthquakes and active tectonics of the Tibetan Plateau and its margins: Royal Astronomical Society Geophysical Journal, v. 99, p. 123–153.

Royden, L., and Burchfiel, C., 1987, Thin-skinned N-S extension within the convergent Himalayan region: Gravitational collapse of a Miocene topographic front, *in* Coward, M., et al., eds., Continental extensional tectonics: Geological Society [London] Special Paper 27, p. 611–619.

Seeber, L., and Gornitz, V., 1983, River profiles along the Himalayan arc as indicators of active tectonics: Tectonophysics, v. 92, p. 335–367.

Tanimoto, T., 1998, State of stress within a bending spherical shell and its implications for subducting lithosphere: Geophysical Journal International, v. 134, p. 199–206.

Wesnousky, S., Kumar, S., Mohindra, R., and Thakur, V., 1999, Holocene slip rate of the Himalayan frontal thrust of India: Observations near Dehra Dun: Tectonics, v. 18, p. 967–976.

Zoback, M., 1992, First- and second-order patterns of stress in the lithosphere: The world stress map project: Journal of Geophysical Research, v. 97, p. 11 703–11 728.

Manuscript received November 6, 2000
Revised manuscript received April 19, 2001
Manuscript accepted May 10, 2001

Printed in USA